

# Optical Localization of a Mobile Robot Using Sensitivity-based Data Fusion

Jason N. Greenberg and Xiaobo Tan

**Abstract**—Optical communication is of increasing interest as an alternative to acoustic communication for robots operated in underwater environments. Our previous work presented a method for LED-based Simultaneous Localization and Communication (SLAC) that uses the bearing angles, obtained in establishing line-of-sight (LOS) between two beacon nodes and a mobile robot for communication, for geometric triangulation and thus localization of the robot. In this paper, we consider the problem of optical localization in the setting of a network of beacon nodes, and specifically, how to fuse the measurements from multiple pairs of beacon nodes to obtain the target location. A sensitivity metric, which represents how sensitive the target estimate is with respect to the bearing measurement errors, is used for selecting the desired pair of beacon nodes. The proposed solution is evaluated with extensive simulation and preliminary experimentation, in a setting of three beacon nodes and one mobile node. Comparison with an average-based fusion approach and an approach using a fixed pair of beacon nodes demonstrates the efficacy of the proposed approach.

## I. INTRODUCTION

When working in a group, an individual agent can use the data shared among the group to localize itself relative to the other agents in a collaborative manner. Triangulation, which uses angles relative to several neighbors with known positions, often referred to as beacons (or base nodes), is one of several position-measuring techniques used in these collaborative settings [1].

In their comprehensive review of the vast field of triangulation, Pierlot and Van Droogenbroeck distinguish four general categories, Geometric Triangulation, Geometric Circle Intersection, Iterative methods, and Multiple Beacons Triangulation, with Geometric Circle Intersection being noted one of the more popular approaches [2]. In this particular type of triangulation, the bearing angles between two beacons and a target are used to describe an arc that spans the beacons and also contains all possible positions of the target. A second arc, created by the addition of a third beacon, allows for an intersecting point to be deduced. However, this approach often has conditions in terms of various angles and orientations of the beacons as well as numerous other conditions for the procedure to work [2], [3].

Group-based localization approaches have the benefit of being operational in typical GPS-denied environments such as indoors and underwater. Underwater implementations traditionally rely on acoustic signals which are notorious for

Jason N. Greenberg and Xiaobo Tan are with the Smart Microsystems Laboratory, Department of Electrical and Computer Engineering, Michigan State University, East Lansing, MI, 48824 USA e-mail: green108@egr.msu.edu (J.N.G.), xbtan@egr.msu.edu (X.T.).

This work was supported by the National Science Foundation (ECCS 1446793, IIS 1734272).

low data rates and low signal reception reliability due to their limited bandwidth, long propagation delays, and multipath effect [4]–[7]. Optical communication systems such as those based on Light-Emitting Diodes (LEDs) are becoming viable alternatives to acoustic-based methods. However, LED-based approaches require a near line of sight (LOS) between transmitter and receiver, though this has been addressed in several ways, including the use of redundant transmitters/receivers [8]–[11] and active alignment [12]–[14].

In our earlier work, [15] and [16], an LED-based optical system was proposed as a solution to Simultaneous Localization and Communication (SLAC). Localization was achieved by using two base nodes (or beacons) with known positions to capture the bearing angles needed to establish optical LOS between these base nodes and a mobile robot. These angles were then used to triangulate the robot's coordinates. To help maintain LOS between the two sides despite the mobility of the robot, a Kalman filter was implemented to predict the robot's future positions, allowing the system to localize dynamically. A noticeable limitation of this two-base-node method is the singularity issue when the mobile node approaches a collinear configuration with the base nodes.

In this paper we consider the problem of optically localizing a mobile robot with a group (more than two) of base nodes. This problem is motivated by not only the aforementioned singularity issue, but also the scenario of sensor networks, where the locations of multiple nodes (stationary or mobile) are known, which provides redundancy in localization. A key question is how to effectively fuse the bearing angle information available from these multiple base nodes. We propose to exploit a sensitivity metric to select the best (most robust) pair of base nodes for triangulation at each time. In particular, the metric describes how sensitive the triangulated position is with respect to the bearing measurement errors. The chosen pairing is then used to compute the target's position using the corresponding measured bearings, which is then fed into a Kalman filter for prediction of the robot's next position. The latter prediction is critical for facilitating the LOS establishment for next round of communication and localization [15] and [16].

The proposed method is evaluated with extensive simulation and preliminary experimentation using a three-base-node implementation. Simulation compares the performance of the proposed approach against two alternative methods when the measurement angles are subject to varying levels of noise. The alternative approaches include the two-base-node approach from [15] and [16] and a method that uses

the average of triangulated target positions based on bearing measurements from all possible pairs of base nodes. Results show that the proposed sensitivity metric-based approach outperforms both alternatives and achieves an average estimated position error of roughly 1 grid unit across all levels of measurement noise. Preliminary experimentation results support the success noticed in simulation and illustrates the proposed method's implementation in hardware.

The remainder of this paper is organized as follows. Section II reviews the position triangulation technique and Kalman filtering for the setting of two base nodes and one mobile node (target). Section III details the sensitivity metric and the proposed fusion approach. Simulation results are provided in Section IV, followed by experimental evaluation in Section V. Finally, conclusion and future work are discussed in Section VI.

## II. REVIEW OF THE TWO-BASE-NODE LOCALIZATION APPROACH

### A. Measurement Process

The proposed approach considers the two-dimensional (2D) setting. Although extension to 3D is conceptually straightforward, hardware implementation is more involved. For the two-base-node approach, the network is composed of one pair of base nodes (with known locations,  $BN_1$  and  $BN_2$ ) and a mobile node (MN) to be localized, as illustrated in Fig. 1. Bearing angles  $\theta_1$  and  $\theta_2$ , are captured by the respective base node via LOS measurement. With these angles and the locations of the base nodes, the values of the  $x$  and  $y$  coordinates of the mobile node are computed as:

$$\begin{bmatrix} n_x \\ n_y \end{bmatrix} = \begin{bmatrix} B_{1x} + |V_1| \cos \theta_1 \\ B_{1y} + |V_1| \sin \theta_1 \end{bmatrix} \quad (1)$$

where  $[n_x, n_y]^T$  is the position vector of the mobile node MN,  $B_{1x}$  and  $B_{1y}$  are the respective  $x$ - and  $y$ - coordinate for  $BN_1$  and  $|V_1|$  is the magnitude of vector  $V_1$  shown in Fig. 1 and is obtained using the Laws of Sines. In particular,

$$|V_1| = \frac{d \sin(\bar{\theta}_2)}{\sin(\theta_1)} \quad (2)$$

where the value of  $d$  is the distance between  $BN_1$  and  $BN_2$ ,  $\bar{\theta}_2$  is the complement of  $\theta_2$ ,  $\bar{\theta}_2 = 180^\circ - \theta_2$ , and  $\theta_n$  is the angle corresponding to the side  $BN_1-BN_2$  within the  $MN-BN_1-BN_2$  triangle,  $\theta_n = \theta_2 - \theta_1$ .

It is assumed that each node in the network is equipped with an optical transceiver comprised of an LED transmitter and a photodiode receiver, and that this transceiver is able to rotate a full  $360^\circ$ . Furthermore, the node is able to identify at any particular moment the angle at which its transceiver is facing with respect to a reference direction such as the east axis identified by a magnetic compass.

Although this process seems straightforward, it is particularly challenging when the target is mobile, since this often results in insufficient synchronization and coordination among all of the nodes to produce proper LOS measurements. There is also the inherent trouble of dealing with errors in the measurement angles, which is problematic since

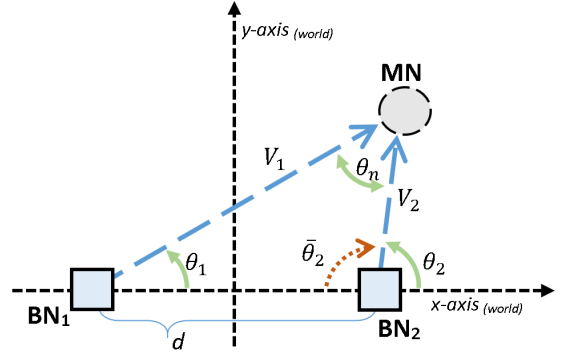


Fig. 1. Illustration of the geometric triangulation used in the two-base-node approach.

the position is obtained via pure algebraic calculation (1) and the noise in the angles will lead to highly variable (instead of smooth) estimated trajectories for the mobile node MN. This issue is addressed with Kalman filtering, by exploiting the predicted positions of the MN it generates from measurements computed by (1), to significantly reduce the effort of searching for the LOS and thus enabling efficient and accurate localization. The Kalman filtering algorithm is presented next.

### B. The Kalman Filtering Algorithm

The mobile node's dynamics are assumed to be adequately represented with a constant velocity model corrupted with Gaussian noise, as it is unlikely that the base nodes would have precise knowledge of mobile node's movement beforehand. Although other filtering schemes could have been potentially used, this assumption on the dynamics enables the use of computationally efficient Kalman filtering for predicting the mobile node's coordinates. These dynamics for the mobile node can be represented as:

$$\mathbf{n}_{k+1} = \mathbf{n}_k + \mathbf{v}_k \Delta_k + w_{1,k} \quad (3)$$

$$\mathbf{v}_{k+1} = \mathbf{v}_k + w_{2,k} \quad (4)$$

where  $\mathbf{n}_k = [n_{x,k}, n_{y,k}]^T$  and  $\mathbf{v}_k = [v_{x,k}, v_{y,k}]^T$  are the position and velocity vectors of the mobile node at the  $k$ -th iteration,  $w_{1,k}$  and  $w_{2,k}$  are independent, zero-mean, white Gaussian noises, and  $\Delta_k$  is the  $k$ -th sampling interval. The noise-corrupted location observation,  $\mathbf{z}_k$ , is represented as:

$$\mathbf{z}_k = \mathbf{n}_k + w_{3,k}, \quad (5)$$

where  $w_{3,k}$  is assumed to be a white, zero-mean Gaussian noise, and independent of the process noises  $w_{1,k}$  and  $w_{2,k}$ . The Kalman filter can then be used to predict and estimate the state vector, consisting of the position and velocity of the mobile node [16].

At time  $k$ , each of the base nodes in the system performs a search for the angular location of the mobile node. The captured angles are combined to generate the observation  $\mathbf{z}_k$  to be used in the state estimate update. The angular search process for each  $i$ -th base node is centered about an anticipated value of that nodes' angular location  $\theta_i$  to

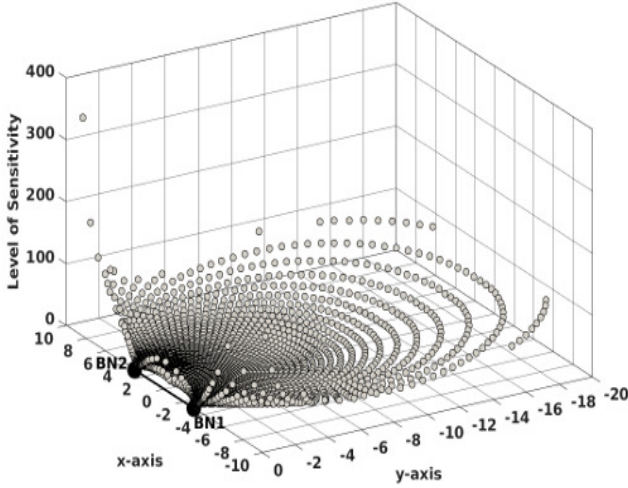


Fig. 2. Illustration of the spatial sensitivity of the two-base-node measurement function.

the MN (recall Fig. 1). The anticipated angle for the  $i$ -th base node,  $\hat{\theta}_{i,k}$  is computed from the position component,  $\hat{n}_x^-, \hat{n}_y^-$ , of the predicted state estimate  $\hat{\mathbf{x}}_k^-$  as follows:

$$\hat{\theta}_{i,k} = \cos^{-1} \left( \frac{\mathbf{V}_b \cdot \mathbf{V}_{m_i}}{|\mathbf{V}_b| |\mathbf{V}_{m_i}|} \right) \quad (6)$$

where,

$$\mathbf{V}_b = \begin{bmatrix} 1 \\ 0 \end{bmatrix}, \quad \mathbf{V}_{m_i} = \begin{bmatrix} \hat{n}_x^- \\ \hat{n}_y^- \end{bmatrix} - \begin{bmatrix} B_{ix} \\ B_{iy} \end{bmatrix} \quad (7)$$

Here  $[B_{ix}, B_{iy}]^T$  are the position coordinates of the  $i$ -th base node  $BN_i$ . The mobile node, in the meantime, will use its predicted position to calculate the angular locations of the base nodes relative to itself, and focus its light along these angles during the angular search.

### III. SENSITIVITY METRIC

When there are more than 2 base nodes (in the 2D setting), the question arises as to how to best utilize the information available from all base nodes. This paper proposes the use of a sensitivity metric that is able to characterize the level of uncertainty of a computed position in terms of the level of uncertainty in the measured bearing angles. In particular, the infinity norms of the Jacobian in the  $x$  and  $y$  direction,  $\|J_x\|_\infty$  and  $\|J_y\|_\infty$ , respectively, of the measurement equation (1) with respect to angles  $\theta_1$  and  $\theta_2$  are used to construct the sensitivity metric.  $\|J_x\|_\infty$  and  $\|J_y\|_\infty$  are computed from  $f_x(\theta_1, \theta_2)$  and  $f_y(\theta_1, \theta_2)$ , which represent the measurement equation (1) in terms of the measurement angles, as follows:

$$\begin{aligned} \|J_x\|_\infty &= \left\| \frac{\partial f_x}{\partial \theta_1} \quad \frac{\partial f_x}{\partial \theta_2} \right\|_\infty \\ &= \frac{2}{d} \left| \frac{1}{\sin^2(\theta_2 - \theta_1)} \right| \max(|\sin 2\theta_2|, |\sin 2\theta_1|) \end{aligned} \quad (8)$$

$$\begin{aligned} \|J_y\|_\infty &= \left\| \frac{\partial f_y}{\partial \theta_1} \quad \frac{\partial f_y}{\partial \theta_2} \right\|_\infty \\ &= d \left| \frac{1}{\sin^2(\theta_2 - \theta_1)} \right| \max(|\sin^2 \theta_2|, |\sin^2 \theta_1|) \end{aligned} \quad (9)$$

These functions characterize how small changes in the measurement angles for a given pair of base nodes result in changes to the computed position. A visual representation of this for a range of positions within  $x \in [-10, 10]$  and  $y \in [0, -20]$  is shown in Fig. 2 for the  $(BN_1, BN_2)$  pair. In this plot the  $z$ -axis indicates the level of sensitivity, calculated as the Euclidean norm of  $(\|J_x\|_\infty, \|J_y\|_\infty)$ .

During system implementation, after all of the base nodes are finished with their scans, each base node pair combination uses their captured angles to evaluate the magnitude of  $J = (\|J_x\|_\infty, \|J_y\|_\infty)$ , which is the sensitivity metric. The base node pairing with angles that produce the lowest sensitivity level is used to compute the value of  $z_k$ , which is subsequently used in the Kalman filtering for position estimation and prediction.

## IV. SIMULATION RESULTS

Extensive simulation was conducted to examine robustness of the proposed approach and two alternative schemes when dealing with various levels of angle measurement noise. The alternative methods included an averaging approach where the measured locations by all base node pairings are averaged, and an approach that uses a fixed pair of base nodes.

### A. Simulation Setup

Although our approach applies to a network of arbitrary number of base nodes, the simulation presented here used a setting with 3 base nodes. The locations of the three base nodes,  $BN_1$ ,  $BN_2$ , and  $BN_3$ , were  $[-3, -3]^T$ ,  $[0, 0]^T$ , and  $[3, -3]^T$ , respectively. This configuration is illustrated in Fig. 3, along with the mobile node's planned trajectory for the simulation. The trajectory consists of 235 position points represented in the figure by the small circles, with the first and last points overlapping at  $[-1, -6]^T$ . In the figure, the base nodes are represented by the three square shapes in the center, and the mobile node is represented by a larger shaded-in circle and is located at the first position of the trajectory.

In the absence of physical LED and photodiode components, certain aspects of the experiment were emulated in the simulation. In particular, techniques were developed for detecting when two nodes can establish LOS for communication and angle measurement, emulating occlusions due to another base node blocking the LOS, and simulating measurement angle errors. In particular, angle measurement errors were mimicked by adding independent, zero-mean, white Gaussian noises to each of the ground truth angles, corresponding to the base nodes that were able to establish LOS with the MN during the measurement sequence. The level of angle error was controlled by changing the standard deviation of the Gaussian noise.

### B. Simulation Results: Impact of Angle Measurement Error

The localization performance was analyzed under different levels of angle measurement error by ranging the standard

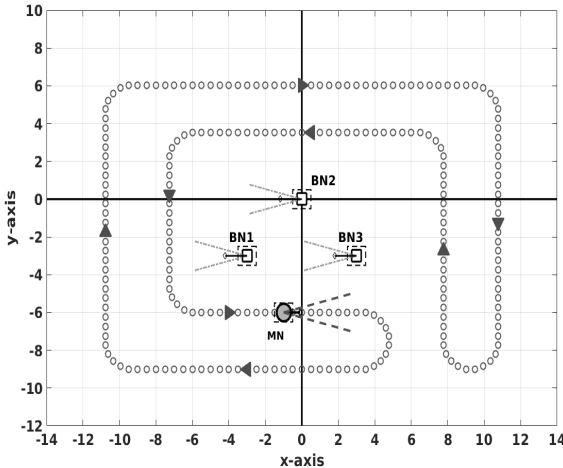


Fig. 3. Base Node configuration and Mobile Node trajectory used in simulation.

deviation of the Gaussian noise from  $0.5^\circ$  to  $5.0^\circ$  in increments of  $0.5^\circ$ . For each level of standard deviation, 100 trials were conducted, with 100 random seeds chosen to ensure the randomness was consistent across each level of standard deviation.

Fig. 4 shows the average measured and estimated errors among all of the trials under each level of standard deviation. The measured (resp., estimated) error is the magnitude of the error obtained by comparing the measured (resp., estimated) positions with the corresponding ground truth position. The average errors shown in Fig. 4 were computed using the mean errors from each trial, which were obtained in each trial by averaging the measured and estimated errors from all of the steps of the trajectory the system had reached during that trial. A noticeable trend in the simulation results is that the average number of consecutive positions in the trajectory that the system was able to reach decreases as the amount of standard deviation in the Gaussian noise increases. This is reflected in Fig. 5, which shows for each standard deviation, the average number of consecutive positions the system was able to reach over the 100 trials. This behavior correlates with the increase in position error relative to the increase in standard deviation to the Gaussian noise as shown in Fig. 4.

Collectively the graphs show that all three methods perform better when the angular measurement error has a lower level of standard deviation. However, each method has a different critical level of standard deviation at which point there is a sharp increase in the position error and sharp decrease in how long the system can track the mobile node. Most notably, the proposed algorithm, which uses the sensitivity metric for data fusion in its measurement scheme, outperforms the two alternative methods, maintaining relatively low levels of position error and is able to reach on average more consecutive trajectory points than the other methods.

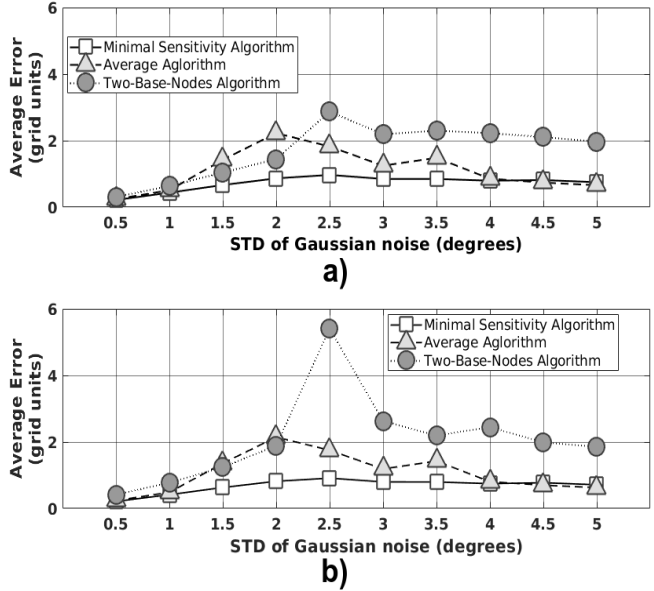


Fig. 4. Average position errors computed among all of the trials for varying amounts of standard deviation in the Gaussian noise added to the angular measurements of the base nodes. Subplot a) shows the average measured error, which is the difference between the observed positions  $\mathbf{z}_k$  and ground truth. Subplot b) shows the average estimated error which is difference between the ground truth and the position from the Kalman filter's state vector  $\hat{\mathbf{x}}_k = [\hat{n}_x, \hat{n}_y]$  after processing the observed position  $\mathbf{z}_k$ .

Another important observation to make, is that the average number of position points the two-base-node approach reaches for all values of the standard deviation is significantly less than the two approaches which used three base nodes. In particular, the average value is capped off at around 60 consecutive points or less. A closer look at the trajectory would indicate that this is roughly the number steps into the trajectory that would take the mobile node to the  $x$ -axis and thus is collinear with its only base node pair.

## V. EXPERIMENTAL RESULTS

### A. Setup

Each node used in the experiment made use of the circular PCB board that housed the transceiver circuitry developed by Al-rubaiai in [13] for processing the light intensity received by the photodiode into a readable analog voltage and enabling quick switching of the LED so to modulate transmitting baud rate of serial communication. The LED (CREE XRE 1 Watt Blue LED, transmitter) and photodiode (Blue Enhanced photodiode, receiver) were connected to the PCB via a removable header-board. The PCB board was mounted to the extended shaft of a stepper motor that passed through the hollow center of a slip ring, thus enabling the transceiver to achieve  $360^\circ$  rotation and still allow the wires connecting the PCB circuit to the embedded controller board to move freely with the rotations. The motor and slip ring were mounted together via a 3D-printed base structure [16].

Each node had an Intel® Edison Board with an Arduino® Expansion Board for the main processing unit. It controlled

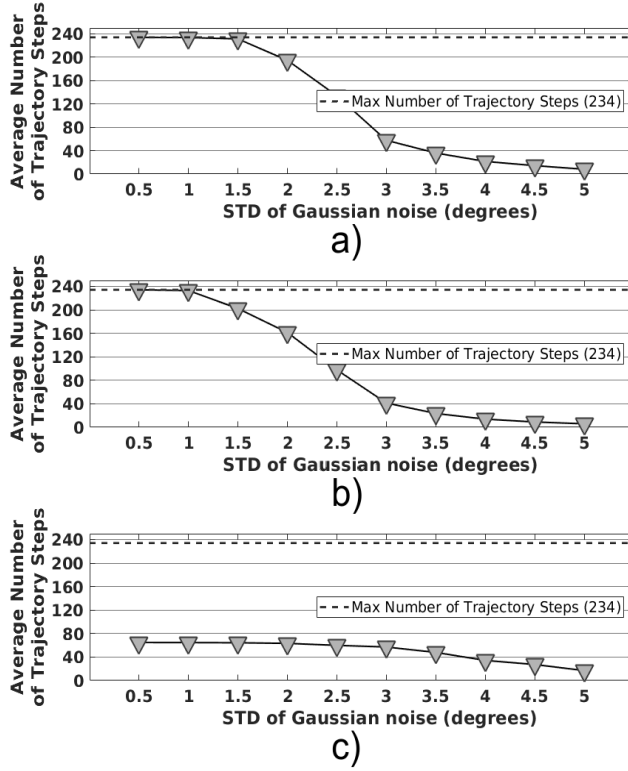


Fig. 5. Line graph showing the average number of consecutive trajectory positions the system is able to reach over the 100 trials for each of the different levels of standard deviation of the Gaussian noise added to the angular measurements of the base nodes, when using each of the measurement scheme: a) the proposed approach using sensitivity metric for data fusion within a three-base node system, b) the alternative three-base node method using position averaging for data fusion c) the two-base node system developed in our previous work.

the rotation of the stepper motor, transmission and reception of the LED signals as well as the processing of the Kalman filter data. A Sparkfun® Big Easy Driver, set to the quarter step mode (i.e. each step rotated the shaft  $0.225^\circ$ ), was used to control the stepper motors by translating step pulses from the Intel® Edison Board to signals readable by the motor step. The orientation of the node's transceiver was maintained by Intel® Edison Board by keeping count of the number steps and their direction that were sent to the driver.

The 3D-printed base was mounted on the top of a Lynxmotion® Aluminum 4WD1 Rover Kit and a 80/20® metal beam, to help maintain the fixed positions, for the mobile node and base nodes, respectively. The mobile node and base nodes are shown in Fig. 6, where they were spread out on the grid structure used for conducting the experiments. The grid structure was laid out on the floor with blue painters tape, where the side length of each square in the grid was approximately 23 cm. While the experiments were conducted in this particular grid, all of the computations relied on the relative grid units. Therefore our method would be generalizable to different physical dimensions due to the scalability of the relative grid units.

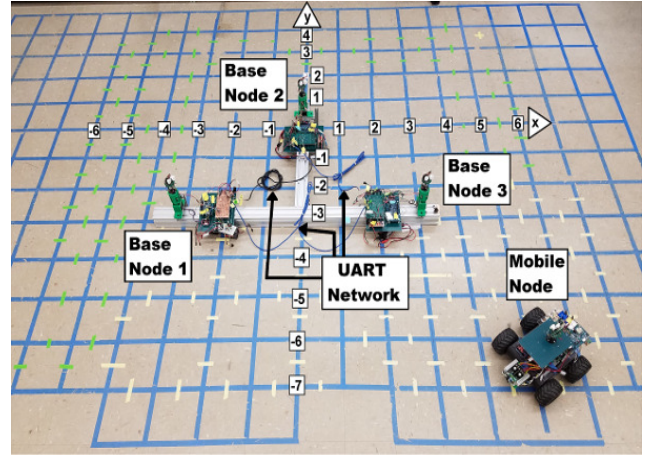


Fig. 6. Overhead view of the grid floor used in experiments.

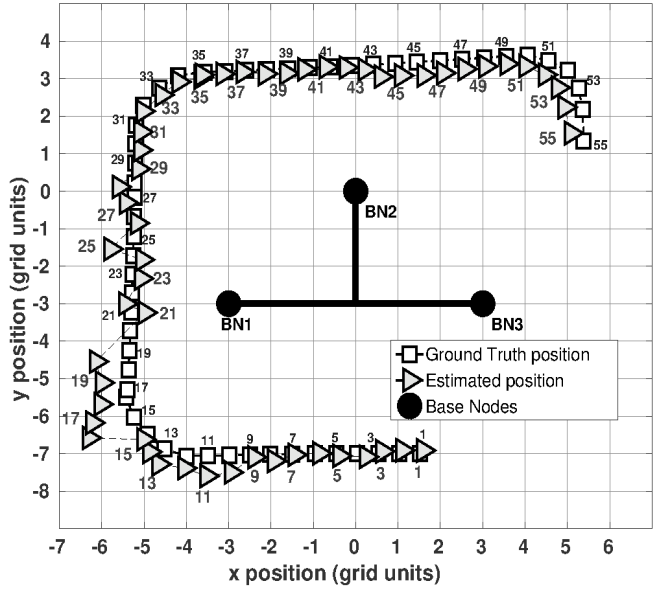


Fig. 7. Experimental results comparing the MN's estimated position against the ground truth.

The Kalman filter computations were done solely on BN<sub>3</sub>; however, because each base nodes captured its own angles independently, the data collected by BN<sub>1</sub> and BN<sub>2</sub> were transmitted back to BN<sub>3</sub> via a physical three-wire Universal Asynchronous Receiver/Transmitter (UART) network. In addition to exchanging angle data, the UART network enabled BN<sub>3</sub> to orchestrate the actions of the other base nodes as well as supply them with the updated state estimates of the MN so each node could search in the appropriate area for the next measurement angle.

The value of the systems' measurement noise covariance matrix,  $R_k$ , was calculated prior to the experiments by having the system try to scan the angles of the mobile node's position while the mobile node remained at a fixed location. The  $x$  and  $y$  errors generated from comparing the base node's measured position against this fixed position were used to

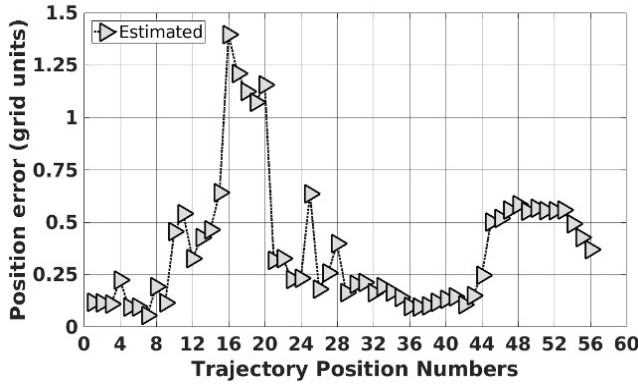


Fig. 8. Experimental results showing MN's estimated position error against trajectory step numbers.

compute the covariance matrix. Because the implementation used in the experiment had 3 base nodes, and then 3 base node pairs, a fixed position in which each pair was forced to measure the location were chosen, with a set of 50 measurements captured for each location. The errors from each of these locations were fused together when generating the covariance matrix so to best characterize the error of this approach.

## B. Results

One preliminary experimental trial of the system was conducted with a trajectory designed to loop around the base nodes in 79 steps. The results of the experiment are shown in Figs. 7 and 8 which compare the estimated and ground truth positions of the mobile node relative to their location within the trajectory and show the estimated position error over the trajectory position number, respectively. Although this single trial only was able to reach 55 of the 79 positions, the results show promise as it is able to use the sensitivity metric to maintain tracking beyond the several instances of being collinear with a pair of the base nodes.

## VI. CONCLUSION

This paper has presented a mobile robot optical localization system that uses a network of multiple beacon nodes. In particular, each node pairing measures bearing angles relative to the robot to compute its position. To optimize the positioning process a sensitivity metric has been proposed, for data fusion of the captured bearing angles from all base nodes. This approach overcomes the limitations of the two-base-node approach and enables a high level of localization accuracy.

Simulated and experimental evaluations were conducted in a two-dimensional terrestrial setting, so to validate the proposed design without the numerous overhead concerns associated with three-dimensions (3D). For future work, we will expand this concept to the 3D setting and explore using more realistic dynamics of the mobile node (rigid-body dynamics instead of point mass dynamics) to enhance

the system performance. Correspondingly, the system hardware will be improved and waterproofed for experimental evaluation in the underwater setting.

## REFERENCES

- [1] J. M. Peula, C. Urdiales, and F. Sandoval, "Explicit coordinated localization using common visual objects," in *2010 IEEE International Conference on Robotics and Automation*, May 2010, pp. 4889–4894.
- [2] V. Pierlot and M. Van Droogenbroeck, "A new three object triangulation algorithm for mobile robot positioning," *IEEE Transactions on Robotics*, vol. 30, no. 3, pp. 566–577, June 2014.
- [3] J. S. Esteves, A. Carvalho, and C. Couto, "Generalized geometric triangulation algorithm for mobile robot absolute self-localization," in *2003 IEEE International Symposium on Industrial Electronics (Cat. No.03TH8692)*, vol. 1, June 2013, pp. 346–351.
- [4] G. Rui and M. Chitre, "Cooperative multi-auv localization using distributed extended information filter," in *2016 IEEE/OES Autonomous Underwater Vehicles (AUV)*, November 2016, pp. 206–212.
- [5] L. Paull, M. Seto, and J. J. Leonard, "Decentralized cooperative trajectory estimation for autonomous underwater vehicles," in *Intelligent Robots and Systems (IROS 2014), 2014 IEEE/RSJ International Conference on*, September 2014, pp. 184–191.
- [6] L. E. Emokpae, S. DiBenedetto, B. Potteiger, and M. Younis, "Ureal: Underwater reflection-enabled acoustic-based localization," *IEEE Sensors Journal*, vol. 14, no. 11, pp. 3915–3925, November 2014.
- [7] A. S. Gadre, D. K. Maczka, D. Spinello, B. R. McCarter, D. J. Stilwell, W. Neu, M. J. Roan, and J. B. Hennage, "Cooperative localization of an acoustic source using towed hydrophone arrays," in *2008 IEEE/OES Autonomous Underwater Vehicles*, October 2008, pp. 1–8.
- [8] D. Anguita, D. Brizzolara, and G. Parodi, "Building an underwater wireless sensor network based on optical: Communication: Research challenges and current results," in *2009 Third International Conference on Sensor Technologies and Applications*, June 2009, pp. 476–479.
- [9] ———, "Optical wireless communication for underwater wireless sensor networks: Hardware modules and circuits design and implementation," in *OCEANS 2010*, September 2010, pp. 1–8.
- [10] I. C. Rust and H. H. Asada, "A dual-use visible light approach to integrated communication and localization of underwater robots with application to non-destructive nuclear reactor inspection," in *Robotics and Automation (ICRA), 2012 IEEE International Conference on*, May 2012, pp. 2445–2450.
- [11] J. A. Simpson, B. L. Hughes, and J. F. Muth, "Smart transmitters and receivers for underwater free-space optical communication," *IEEE Journal on Selected Areas in Communications*, vol. 30, no. 5, pp. 964–974, June 2012.
- [12] P. B. Solanki, M. Al-Rubaiai, and X. Tan, "Extended Kalman filter-aided alignment control for maintaining line of sight in optical communication," in *2016 American Control Conference*, July 2016, pp. 4520–4525.
- [13] M. Al-Rubaiai, "Design and development of an LED-based optical communication system," Master's thesis, Michigan State University, 2015.
- [14] P. B. Solanki, M. Al-Rubaiai, and X. Tan, "Extended Kalman filter-based active alignment control for LED optical communication," *IEEE/ASME Transactions on Mechatronics*, vol. 23, no. 4, pp. 1501–1511, August 2018.
- [15] J. N. Greenberg and X. Tan, "Efficient optical localization for mobile robots via Kalman filtering-based location prediction," in *Proceedings of the ASME 2016 Dynamic Systems and Control Conference*, Minneapolis, MN, October 2016, DSCC2016-9917.
- [16] ———, "Kalman filtering-aided optical localization of mobile robots: System design and experimental validation," in *Proceedings of the ASME 2017 Dynamic Systems and Control Conference*, Tysons, VA, October 2017, DSCC2017-5368.